Climate Dynamics (2023) 61:2735–2751
https://doi.org/10.1007/s00382-023-06709-7

A dominant mode in the first phase of the Asian summer monsoon rainfall: role of antecedent remote land surface temperature

Subodh Kumar Saha[1] · Yongkang Xue[2] · Sujith Krishnakumar[1] · Ismaila Diallo[3] · Yashas Shivamurthy[1] · Tetsu Nakamura[4] · Qi Tang[5] · Hemantkumar S. Chaudhari[1]

Received: 7 November 2022 / Accepted: 7 February 2023 / Published online: 24 February 2023

Abstract

The first/initial phase (during May to June) of the Asian summer monsoon (ASM), primarily driven by land-sea thermal gradient, varies from year to year and enormously affects people's livelihood and the economy of this region. Moreover, the first phase, associated with the sub-seasonal variability (days to weeks), witnesses many extreme hydroclimatic events. Therefore, it is crucial to understand the sources of predictability of the initial phase of the ASM. Here we identify a dominant mode of variability in June rainfall over the entire Asian monsoon region. This mode is found to be linked with the spring (April, May) land surface temperature (LST) of the areas centred around the Western Third Pole (WTP). The Third Pole is the high elevation area centred on the Tibetan plateau. The WTP region is also home to many glaciers and steep mountains, including the second-highest peak in the world (i.e. Karakorum range). Consequently, spring LST has a strong inverse relationship with snow water equivalent ($r = -0.65$) over WTP, suggesting a seminal role of land surface processes in the first phase of ASM variability. The observed dominant modes and their teleconnections are also investigated in the 30-years re-forecast by five global coupled climate models participating in the "Impact of Initialized Land Surface Temperature and Snowpack on Sub-seasonal to Seasonal Prediction phase I" project (LS4P-I; Xue et al. (Geosc Model Devel 14(7):4465–4494, 2021; Bul Amer Meteor Soc 103: E2756-E2767, 2022)). While most models faithfully reproduce the observed link of June rainfall over South Asia with the remote LST, all models fail to capture the same over east Asia. In general, models show a significant bias in simulating the LST and the dominant modes of rainfall variability. Our findings may improve the understanding of the Asian summer monsoon variability and predictability, which may help improve the dynamical sub-seasonal to seasonal forecast system.

Keywords Asian summer monsoon · First phase of monsoon · Land surface processes

✉ Subodh Kumar Saha
subodh@tropmet.res.in

Yongkang Xue
yxue@geog.ucla.edu

Sujith Krishnakumar
sujith@tropmet.res.in

Ismaila Diallo
idiallo.work@gmail.com

Yashas Shivamurthy
yashas.shivamurthy@tropmet.res.in

Tetsu Nakamura
te2nakamur@met.kishou.go.jp

Qi Tang
tang30@llnl.gov

Hemantkumar S. Chaudhari
hemantkumar@tropmet.res.in

[1] Indian Institute of Tropical Meteorology, Dr. Homi Bhabha Road, Pune 411008, India

[2] University of California, Los Angeles, CA 90095, USA

[3] Department of Meteorology and Atmospheric Science, The Pennsylvania State University, University Park, State College, PA 16802, USA

[4] Climate Prediction Division, Japan Meteorological Agancy, Minato, Japan

[5] Lawrence Livermore National Laboratory, Livermore 94550, CA, USA

1 Introduction

The Asian summer monsoon (ASM) is one of the most prominent events in the Earth's climate system, which brings a tremendous amount of moisture from thousands of kilometres across the Indian and Pacific Oceans and produces heavy rainfall over the south and east Asia, including the surrounding oceanic regions. The seasonal migration of the solar insolation in association with land-sea distribution and elevated terrain of the Third Pole (TP; the high elevation area centred on the Tibetan plateau) makes the ASM unique among all other monsoons on the planet. About 60% of the global population lives in the Asian monsoon region, and summer monsoon rainfall enormously contributes to their livelihood and culture. Monsoon rainfall also varies on the sub-seasonal to the decadal time scale (e.g. Yang and Lau 2006; Goswami 2012; Wang et al. 2018), which significantly affects agriculture and the economy (Rosenzweig and Binswanger 1993; Subash and Gangwar 2014). Therefore, a reliable prediction of the ASM has been a core objective of many global/regional forecasting agencies for many years. Despite long efforts, a reliable prediction of monsoon rainfall remained elusive (Shukla 2007).

The scientific basis for higher predictability of tropical climate compared to that of mid and high latitude was laid in the pioneering studies by Charney and Shukla (1981) and generalized by Shukla (1981), Shukla (1998). Therefore, a large number of studies have explored the role of the slowly varying oceanic conditions (e.g. El Niño-Southern Oscillation (ENSO), Pacific Decadal Oscillation (PDO), Atlantic Multidecadal Oscillation (AMO), Indian Ocean Dipole (IOD)) on the prediction and predictability of tropical weather and climate. However, relatively few studies link weather and climate with land surface conditions as the predictor. Limited observation of land surface and sub-surface conditions is believed to be one of the reasons (e.g. Robock et al. 2000). Recent studies (e.g. Xue et al. 2018) have argued that land surface processes may have an equal contribution to weather and climate variability as in the case of sea surface temperature (SST). The nature of land-atmosphere feedback affecting monsoon rainfall could be local and remote. The remote land surface conditions, such as the Eurasian snow cover anomaly in winter and spring, are known to affect seasonal South Asian (Blanford 1884; Dong and Valdes 1998; Bamzai and Shukla 1999; Kripalani and Kulkarni 1999; Saha et al. 2013; Senan et al. 2016; Saha et al. 2017) and East Asian (e.g. Zhang et al. 2017) summer monsoon rainfall. Moreover, spring rainfall over Iran, Pakistan and Afghanistan is inversely related to the first phase of rain (June–July) over India (Rai et al. 2015). Spring land surface temperature (LST) in the TP and Rocky mountains is also found to be associated with rainfall in the following month of June over the downstream region (i.e. southeastern China and North America; Xue et al. 2012, 2016, 2018; Diallo et al. 2019, 2022). Similarly, several studies involve the role of local feedback on the sub-seasonal monsoon rainfall, which significantly affect the monthly/seasonal monsoon rainfall anomaly (e.g. Saha et al. 2011, 2012; Asharaf and Ahrens 2013).

The extreme rainfall on the sub-seasonal time scale (day to few weeks) is challenging to forecast but essential for saving life and property. Moreover, sub-seasonal components being the building blocks of the monsoon, variability on the sub-seasonal scales caused by land surface processes (i.e. through remote or local feedback) may also contribute to the seasonal rainfall anomaly. Observational evidence suggests that sub-seasonal variability, which is so far considered as noise in the context of seasonal prediction, is predictable and has a significant contribution to the seasonal anomaly of Indian summer monsoon rainfall on inter-annual to multi-decadal time scale (Saha et al. 2019, 2020, 2021). Therefore, improving the simulation of sub-seasonal rainfall statistics in a forecast system is also likely to improve seasonal forecasting skills. Since the predictability of monsoon rainfall remains relatively low, further understanding and improving land surface processes in a model along with correct initialization may improve the forecast skill on the sub-seasonal to seasonal (S2S) time scale.

World Weather Research Program (WWRP) and World Climate Research Program (WCRP) together aim to bring weather and climate research communities to leverage their expertise for improving predictions on S2S timescales (WMO 2013). Motivated by the studies that, spring LST in the high altitude regions of TP and Rocky mountains is associated with rainfall on the following month of June over southeastern China and North America, the Global Energy and Water Exchanges (GEWEX)/Global Atmospheric System Study (GASS) has launched a new initiative called "Impact of Initialized Land Surface Temperature and Snowpack on Sub-seasonal to Seasonal Prediction phase I" (LS4P-I; Xue et al. 2021). This study suggests that surface and sub-surface land temperatures of the TP region may have a global impact (Xue et al. 2022).

The elevated heating from the Tibetan plateau (e.g. Yanai and Wu 2006) and sharp edges of the Himalayas (Boos and Kuang 2010) are crucial for the mean Asian monsoon. The transition from spring to summer monsoon season witnesses dramatic changes in the land surface and atmospheric condition, which vary significantly from year to year. It is plausible that variability in the pre-monsoon land-surface conditions over these regions may alter the surface energy balance and consequently the tropospheric heating, which in turn affects the ASM in its first phase. The first phase of monsoon

potentially can affect the seasonal (JJAS or MJJAS average) anomaly (e.g. Saha et al. 2011)). Therefore, understanding of the variability in the initial phase (i.e. June) has direct implications on the seasonal prediction and predictability of the Asian summer monsoon. Here we show the existence of a dominant mode of variability in the Asian monsoon rainfall during June or May-June. The possible link of this mode with antecedent land surface conditions in the observations is presented. We also use 30 years of re-forecast from five global coupled model outputs participating in the LS4P-I project to validate the observed relationship. The manuscript is organized as follows: section 2 describes the observed data used and methodology adopted for data analysis. Results are described in section 3 and 4. A summary of this study is given in section 5.

2 Data and methods

Gridded surface temperature and precipitation data from Climatic Research Unit Time Series (CRU TS; $0.5° \times 0.5°$; monthly) for 1901–2019 is used (Harris et al. 2020). The monthly indices of ENSO, PDO, AMO and IOD is obtained from the site https://psl.noaa.gov/data/climateindices/list/. Indian summer monsoon onset date over Kerala based on India Meteorological Department's (IMD's) subjective (1901–2005) and objective (1971–2019) criteria are taken from Preenu et al. (2017), PAI et al. (2020). The objective criteria of IMD are based on the daily rainfall of 14 stations over Kerala and the neighbouring area, along with wind field and outgoing longwave radiation over the southeast Arabian Sea. While objective criteria emphasize on the sharp increase in rainfall over Kerala along with the setting up of large-scale monsoon flow and extension of westerlies up to 600 hPa. IMD declares monsoon onset dates operationally in a subjective manner considering the sharp increase in rainfall, its sustenance and associated changes in the atmospheric circulation features. Monthly gridded snow water equivalent (SWE) data for the period 1950–2019 from ERA-land reanalysis is utilized (Muñoz Sabater et al. 2021). Monthly winds, specific humidity and geopotential height data in the vertical pressure levels (1901–2015) are from 20th Century Reanalysis V3 by the NOAA/OAR/ESRL PSL, Boulder, Colorado, USA, from their Web site at https://psl.noaa.gov/data/gridded/data.20thC_ReanV3.html. The daily pressure level atmospheric temperature is from ERA5 reanalysis (1997–2020; Hersbach et al. 2020). CPC Global Unified Gauge-Based Analysis of Daily Precipitation data and daily land surface temperature for the years 1979–2020 provided by the NOAA PSL, Boulder, Colorado, USA, from their website at https://psl.noaa.gov/data/gridded/data.cpc.globaltemp.html. Monthly rainfall (land and Ocean) from GPCP (Adler et al. 2003) for 1979–2020 is also used.

The empirical orthogonal function (EOF) analysis is used to decompose June (and May-June averaged) rainfall over the Asian monsoon region (climatological mean rainfall $\geq 1 mm\, day^{-1}$). The Asian monsoon region defined with this criteria also closely matches several previous studies, where the global monsoon domain is determined based on the annual range of precipitation (see Wang et al. 2012; Saha et al. 2016). The standard regression and correlation analysis are done to find the relationship between the two parameters, while the Fourier harmonic analysis is used to calculate the smooth annual cycle (sum of mean and first three harmonics) of rainfall and temperature time series.

The ensemble-averaged hindcast (8–10 ensemble members) of June rainfall and May 2 m temperature for the period 1981–2010 is used from five Earth System Model (ESM; Table 2) participated in the LS4P-I project (Xue et al. 2021, 2022). About 40 groups worldwide (ESMs, regional climate models, and data groups) have participated in this project. The primary objective was to establish the observed effects of TP surface and sub-surface temperature anomaly in May on the June rainfall over Asia in the multi-model framework. Among the participants, five modeling centres provided monthly 2 m temperature and rainfall for May and June, respectively, for 30 years (1981–2010). The Chinese Meteorological Administration (CMA) provides 2 m air temperature, collected from a large number of stations in the Tibetan plateau, which is considered one of the best data in this region (Han et al. 2019; Diallo et al. 2022). Therefore, for comparison of the model's 2 m air temperature, we merged CMA data over China with CRU data for the rest of the region (both with 0.5° resolution; i.e. CMA data over China for 1981–2010 and CRU data elsewhere).

3 Results

3.1 Mean and variability of rainfall

The ASM can be divided into two major components: the South Asian (or Indian) and East Asian summer monsoon systems. While these two systems are largely independent, there is evidence of mutual interactions (e.g. Wu 2017). The summer monsoon onset begins in early May (June) in East (South) Asia with dramatic changes in the land and atmospheric conditions (e.g. extreme dry to very wet and humid conditions).

The climatological mean (1901–2019) rainfall during May and June is shown in Fig. 1. The East Asian regions and Bangladesh receives more than 100 mm of rain during May alone. The rainfall band extends further towards north and west in June, covering South Asia. As the people of the Asian monsoon region are heavily dependent on

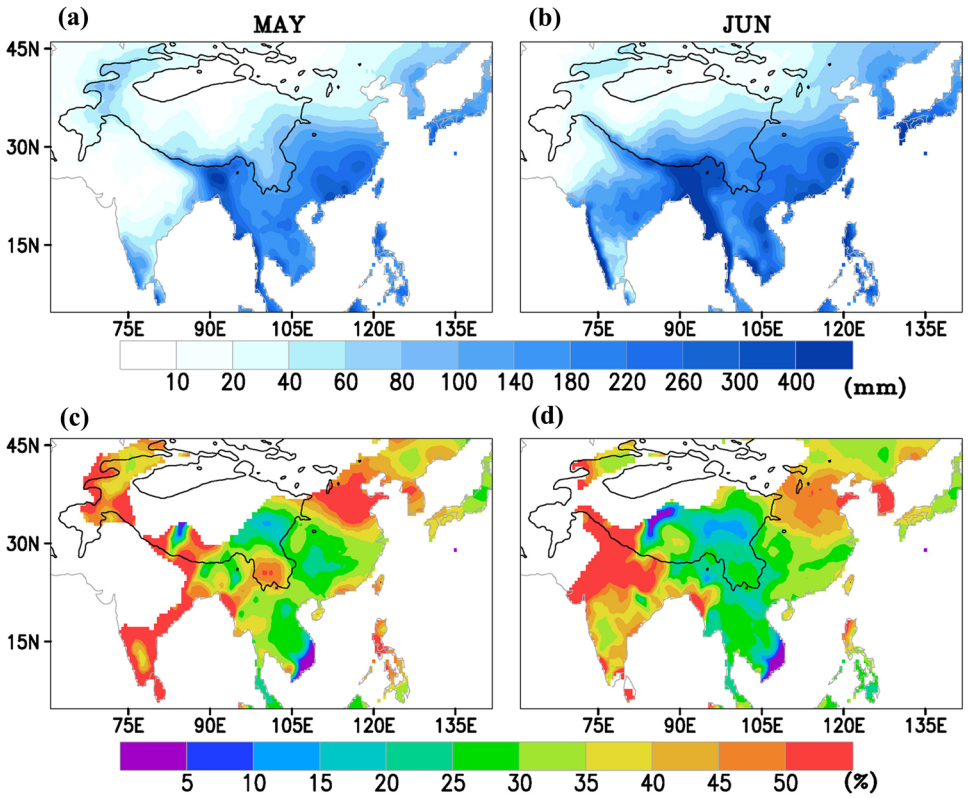

Fig. 1 Climatological mean (1901–2019) monthly rainfall (in mm month^{-1}) during **a** May and **b** June from CRU. The interannual standard deviation of monthly rainfall with respect of mean (in %) during **c** May and **d** June. Areas with rainfall mm day^{-1} is masked out. Height of 1.5 km topography shown by thin black contour

agriculture, the initial phase of monsoon rainfall is crucial for crop sowing. However, the interannual standard deviation of the monthly mean is relatively high over a major part of the monsoon zone (more than 30% of its long term mean; Fig. 1c,d). Moreover, the variability is more substantial over central India (~40–50%). On the other hand, the interannual standard deviation of all India averaged June-to-September rainfall is about 10% of its long term mean (e.g. Krishnamurthy and Shukla 2000; Saha et al. 2021). The mean monsoon onset date in Kerala (a southern state in India) is 1st June, with an interannual standard deviation of about seven days based on combined objectively and subjectively defined dates by IMD in the last 119 years. In the case of the South China Sea (SCS), the mean monsoon onset date varies between 14*and*24*th* May and the interannual standard deviation is about ten days based on various studies (Mao and Chan 2004; Yihui and Chan 2005; Luo and Lin 2017). In fact, large-scale East Asian summer monsoon is characterized by two-stage onset: first over SCS between 16–20 May and another between 14–19 June over Yangtze and Huai River basin, also known as mei-yu (Wang and LinHo 2004). And over the Indochina peninsula, monsoon onset occurs between April and May (e.g. Qian and Lee 2000). Although the onset date varies regionally, the Asian monsoon is a large-scale phenomenon related to land-ocean thermal contrast and processes such as large-scale convection, ocean dynamics, vegetation feedback etc. While the land-ocean temperature gradient drives the monsoon winds/circulation in the very beginning, the convection initiation fueled by the moisture-laden wind increases the tropospheric heating and maintain the monsoon circulation. Therefore, the initiation of rainfall over a major part of the Asian monsoon region is essential for understanding the dynamical aspects of the initial phase of ASM. It is evident from the monthly mean rainfall that the monsoon covers a large part of East Asia during May. Still, it is the month of June when it covers almost the entire Asian monsoon region (including South Asia). Therefore, from the perspective of the large-scale monsoon system, the month of June or May-June average may be considered the initial/first phase of the ASM.

Since the ASM is initially driven by land-sea contrast due to the seasonal migration of the Sun, the year-to-year changes in land surface conditions may also introduce a mode of variability in the first phase of rainfall. In order to find out the existence of any such common mode, EOF analysis is carried out on June rainfall of 119 years (1901–2019; Fig. 2). The first EOF mode (explains 12% of total variance) shows a dipole mode between north and south regions divided by the Yangtze River in China, a very familiar structure of rainfall variation to Xue et al. (2018). On the other hand, the entire Indian sub-continent and Indochina peninsula vary in the same phase. The second and third EOFs explain 7.2% and 6.2% variance, respectively and have a slightly complex structure.

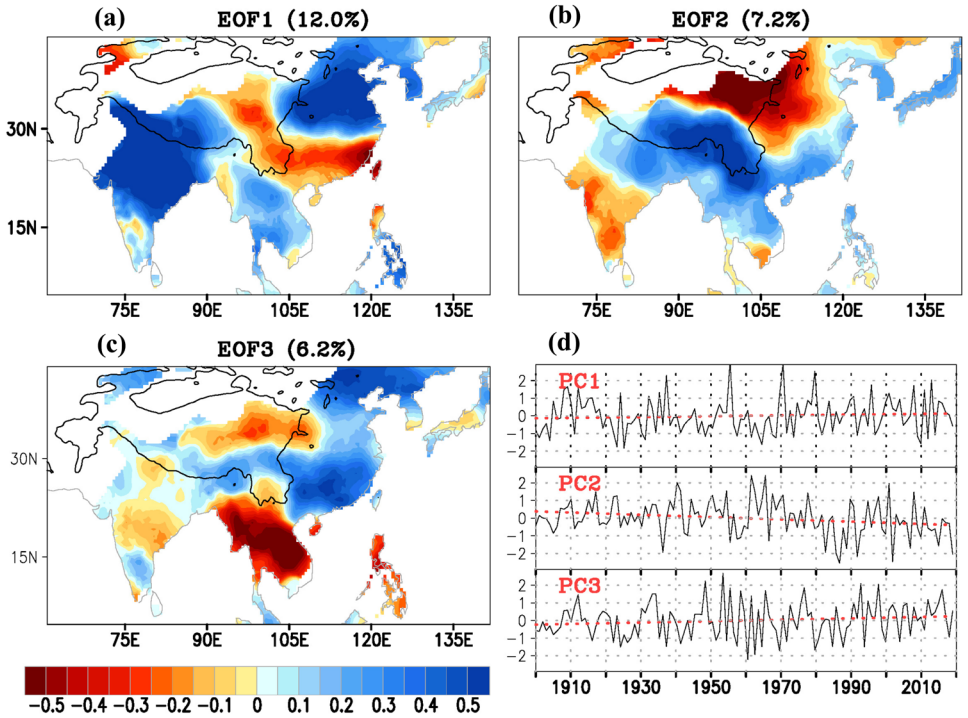

Fig. 2 First three EOFs and PCs of June rainfall from CRU (1901–2019). The percentage of total variance explained by individual EOFs are given in the sub-figure captions

Furthermore, EOF1 is well separated from other EOFs (Figure S01) based on North's significance test (North et al. 1982). Except for the second principal component (PC), which shows a declining trend, PC1 and PC3 do not have a significant trend. Therefore EOF1 appears to be a major natural mode of variability unaffected by long term climate change in the last century.

In general, precipitation variability over land and neighbouring oceans is partially interlinked (or synchronized) owing to the influence of common predictors. Oceanic processes control a large part of rainfall variability on the planet, including land regions (e.g. ENSO, IOD), and a large part of the oceans in the Asian monsoon region also gets intense rainfall. Therefore, a larger weight from the oceanic regions is expected in the dominant mode of EOF of rainfall. Nevertheless, the second EOF using GPCP rainfall (land and ocean; 1979–2019) over the same domain mimics the first EOF pattern obtained from long-term data over land only (Figure S01). Furthermore, the first two EOFs are well separated (based on North's significance test). When PC1 from land-only precipitation is correlated with GPCP rainfall of June, the correlation pattern matches with the EOF2 of GPCP rainfall and EOF1 of CRU rainfall (Figure S01b). We also note that except sub-tropical west Pacific region, the Arabian Sea and Bay of Bengal regions do not show strong variability. Furthermore, EOF1 of May to June averaged precipitation also show a similar structure (Figure S3 a,b), suggesting a robust dominant mode in the first phase of the ASM.

3.2 Teleconnections

Several recent studies have pointed out a link between the initial LST of sub-tropical high altitudes regions, such as TP and Rocky mountain, on rainfall of remote areas (i.e. eastern China, great plain in the USA) on the following month (e.g. Xue et al. 2012, 2016, 2018; Diallo et al. 2019, 2022). Similarly, remote antecedent land surface conditions are found to be associated with the initial phase of south ASM rainfall (Rai et al. 2015). Therefore, it is plausible that the dominant mode of the initial phase of the ASM is also associated with antecedent land surface conditions. Thus, correlation between the first PC and April, May 2 m temperature is calculated. The correlations indeed show a strong association of the first dominant mode in June rainfall with the surface temperature of the areas centered around western TP (WTP) and part of north Sahara (Fig. 3a, b). We also note that a significant negative correlation during May is seen over the Indochina peninsula (ICP). A similar correlation pattern is also found when PC1 of May-June averaged rainfall used (Figure S3 c, d), suggesting robustness in the consideration of the initial phase of ASM.

The WTP region is also known for steep terrain and is home to the world's second-highest peak, the Karakorum Mountain range. This region also remains covered with large glaciers and snow. The correlation between monthly SWE from ERA5-Land and 2 m temperature from CRU TS averaged over WTP box during May is −0.65 (for the years 1950–2019; Fig. 3d). Furthermore, the mean and

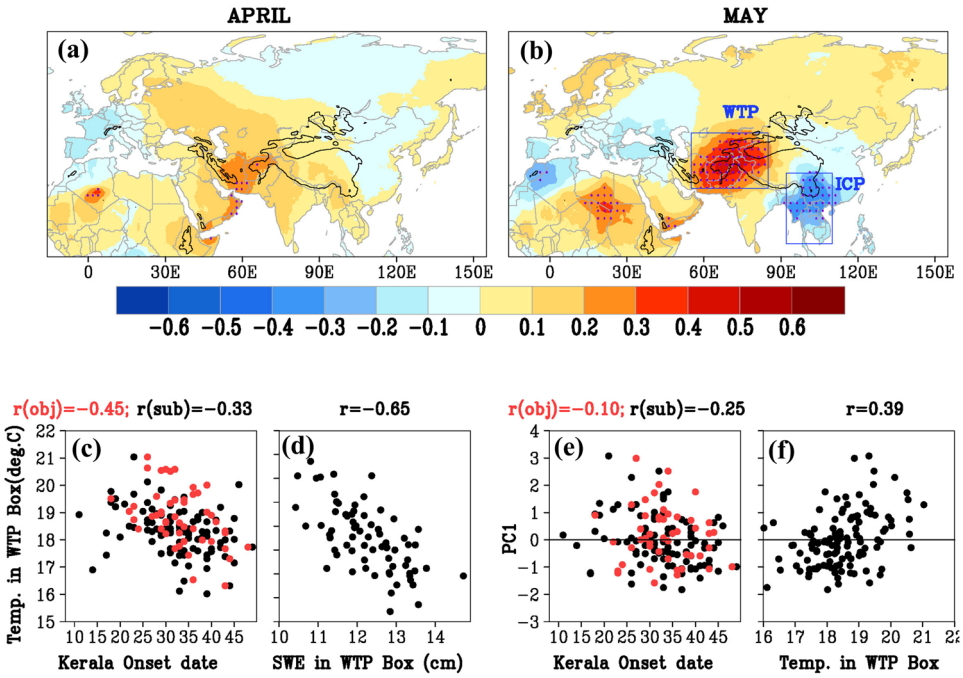

Fig. 3 Linkages of the initial phase of the monsoon variability with land surface parameters. PC1 is correlated (1901–2019) with surface air temperature (2 m) during **a** April and **b** May. The maximum and minimum correlation regions found in May are marked by the rectangle that are defined as regions located around western Tibetan plateau (WTP) and Indochina peninsula (ICP) respectively. Correlations significant at 5% (two-tailed Student's t-test) are stippled. Scatter plot between WTP box averaged temperature and **c** monsoon onset date over Kerala based on IMD's subjective (1901–2005; black dots), objective (1971–2019; red dots) criteria, **d** snow water equivalent averaged over WTP box during May (ERA5-land; 1950–2019). Scatter plot between PC1 and **e** monsoon onset dates over Kerala, **f** temperature averaged over WTP box (correlations above 0.18 are significant at above 95% level using two-tailed Student's t-test)

interannual standard deviation of SWE is 122.5 mm and 8.8 mm, respectively. Therefore, year-to-year variability in snow/ice during spring may induce large variability in the surface energy fluxes due to strong snow-albedo feedback, which in turn may affect the atmospheric circulation. The variability in surface energy flux over the WTP region may also affect the initial build-up of the north–south tropospheric temperature gradient. The summer monsoon onset dates are known to be intimately connected with the north–south tropospheric temperature gradient (e.g. Goswami and Xavier 2005). Therefore, we use the onset date over Kerala (southern tip of India) defined by the IMD and correlated with WTP averaged temperature. The scatter diagram between objectively (subjectively) defined onset date of IMD and WTP average 2 m temperature shows a strong and significant inverse relationship ($r^{wtp}_{obj} = -0.45, r^{wtp}_{sub} = -0.33$ are significant $\geq 99\%$ using two-tailed Student's t-test; Fig. 3c). A significant link between PC1 and onset date over Kerala ($r^{pc}_{sub} = -0.25$ significant at $\geq 99\%$) and WTP temperature ($r^{pc}_{wtp} = 0.39$ significant $\geq 99\%$) further suggests that onset is also a part of the large-scale monsoon system, initially driven by land-surface conditions (Figures 3e, f). Hence, it is very likely that an early (late) onset is linked with warmer (colder) tropospheric temperature in association with warm (cold) WTP surface.

Mountains (e.g. Himalayas) are known sources of stationary waves. Moreover, strong temperature anomaly over high mountain regions in the WTP may also trigger stationary eastward propagating Rossby wave train (e.g. Ringler and Cook 1999), affecting rainfall/surface conditions over remote areas. In order to examine the possibility that such a stationary wave exists, May WTP temperature and PC1 of June rainfall are regressed with geopotential height at 200 hPa from NOAA-CIRES-DOE 20th Century Reanalysis (1901–2015). The regressed geopotential height shows a stationary wave pattern moving around the globe (Fig. 4). The regression pattern using PC1 of June rainfall is quite similar to that with WTP LST during May (Fig. 4a, c) It is also noted that the regressed values over WTP and northeast of China are in opposite phases. This implies an antiphase relationship in rainfall variability between India and south of the Yangtze River, that is consistent with the pattern found in EOF1 of June (or May–June) rainfall (shown in Fig. 2). Moreover, the maxima of the regression values lie over WTP, with opposite phases around the Rocky Mountain region, suggesting a possibility of weather and climate in

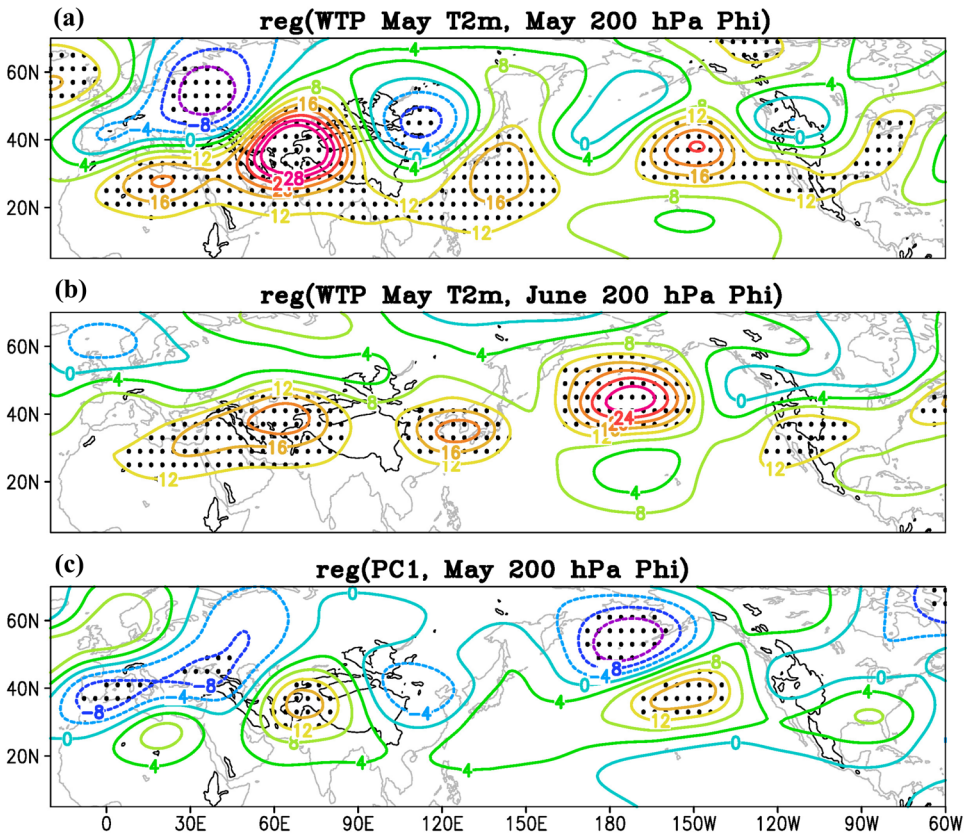

Fig. 4 WTP averaged CRU LST of May is regressed with geopotential height at 200 hPa from NOAA-CIRES-DOE 20th Century Reanalysis V3 (1901–2015) during the month of **a** May and **b** June. **c** PC1 of June rainfall is regressed with geopotential height at 200 hPa during May. The thin black contour represents topography at 1.5 km height, regression significant at 90% are stippled

North America being affected (e.g. Xue et al. 2022). The associated wave pattern is also evident in the regression of geopotential height in June (Fig. 4b). The wave activity flux during positive and negative years (based on WTP May LST; shown in Fig. 7a further suggest eastward propagation of stationary wave (Figure S4). It is plausible that land anomalous surface conditions over WTP may trigger eastward stationary wave.

Elevated surface heating over the Tibetan plateau region is known to have a major impact on the Asian summer monsoon (Yanai et al. 1992). In the early spring, LST begins to rise and land surface heats up the overlying atmosphere and helps to increase the tropospheric temperature gradient (TTG). The north–south TTG drives the low-level winds and consequently initiates the low-level moisture convergence during the initial phase of the monsoon. Once convection begins, the latent heat release due to precipitation further increases the upper-level atmospheric temperature, enhancing the north–south TTG. Therefore, TTG is related to the strength of the monsoon rainfall, and some studies use the TTG index to identify the onset and withdrawal date of the Indian summer monsoon (e.g. Goswami and Xavier 2005; Xavier et al. 2007).

Since the surface temperature of the WTP region shows a strong association with the monsoon rainfall, local land surface heating may have affected the tropospheric temperature and, consequently, the moisture fluxes. To investigate this, WTP averaged CRU surface temperature during May is correlated (regressed) with the tropospheric temperature (vertically integrated moisture fluxes) by employing NOAA's 20th Century Reanalysis (1901–2015). Here, air temperature average of 600–200 hPa is considered as tropospheric temperature, and the vertical integration of moisture fluxes (qu, qv) is done from the surface to 200 hPa. It turns out that surface temperature over WTP in May has a strong and significant correlation with the tropospheric temperature of the sub-tropical region (15–50N; Fig. 5a, b) during May and June. Similarly, regressed moisture flux shows cyclonic circulation over India, ICP regions and anti-cyclonic circulation south of the Yangtze River, supporting the precipitation structure of the first EOF. While the regressed moisture flux pattern and TTG are quite persistent from May to June (i.e. Fig. 5), the relationship during July becomes rather weak and insignificant (figure not shown). We also note that in the WTP region, the surface temperature is strongly correlated with the tropospheric temperature during May (i.e. simultaneous), but becomes weaker and rather widespread around west Asia during June (i.e. in one month lead). As PC1 of June rainfall is significantly correlated with May WTP LST, regression/correlation using PC1 also shows a similar structure (figure not shown).

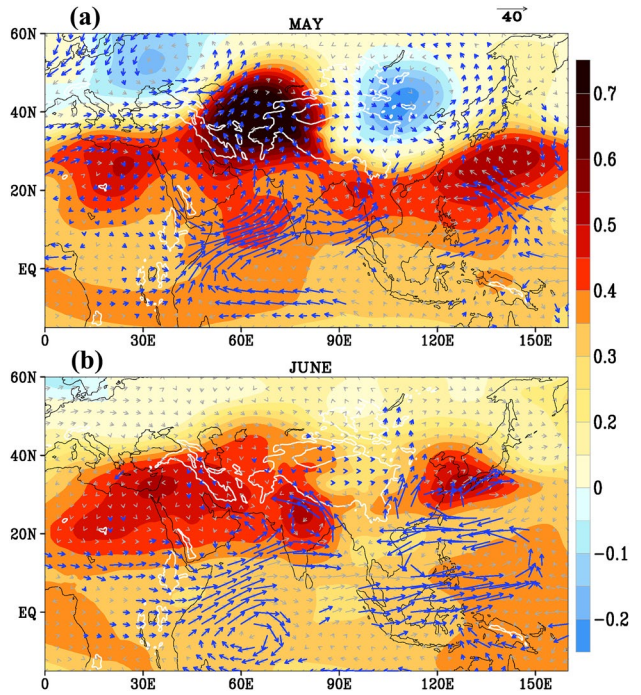

Fig. 5 Relationship of WTP surface temperature with large scale tropospheric temperature (average of 600–200 hPa) and vertically integrated moisture fluxes (surface to 200 hPa). WTP averaged surface temperature during May is correlated (regressed) with tropospheric temperature (moisture flux) of the month **a** May and **b** June. Correlations (shaded plot) above 0.18 are significant at above 95% level. Regressed moisture fluxes (vectors) significant at above 95% are marked by blue colors

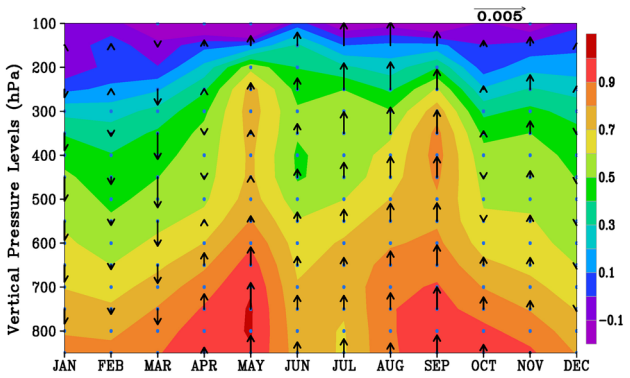

Fig. 6 Association of monthly WTP land surface temperature with the overlying atmospheric temperature and vertical velocity. Monthly WTP surface temperature is correlated (regressed) with the air temperature and Omega in the vertical levels (1901–2015; CRU LST and NOAA's 20C Reanalysis temperature, Omega). Correlations (shaded) significant at above 95% are stippled and arrows represents direction of regressed vertical velocity

While local surface sensible heating may trigger anomalous ascending motion and heats up the troposphere, it is also possible that strong tropical/sub-tropical convection remotely may create anomalous dry and warm surface conditions through large-scale subsidence Rodwell and Hoskins (1966). To verify the possibilities, simultaneous correlation (regression) between monthly WTP surface temperature and vertical levels of atmospheric temperature (vertical velocity; Omega) is calculated. As negative Omega represents ascending motion, in this analysis sign of Omega is reversed to represent positive (negative) regression value as ascending (descending) motion through arrow marks. Therefore, the upward (downward) direction of the regressed Omega anomaly suggests an ascending (descending) motion. A strong, significant and positive correlation with a maximum in the lower side of the atmosphere during Spring (March to May) and late summer to early Autumn (August to October) is evident (Fig. 6). The maxima in the regressed upward Omega in the lower troposphere coincide with the correlation maxima. Moreover, an increasing correlation since early spring in the lower part of the atmosphere and the upward direction of regressed Omega suggests possible heating of the atmosphere by land surface processes. While Omega decreases during June-July and again picks up in September in the lower levels, a stronger anomaly in the upper atmospheric levels also suggests the role of large-scale remote influences through the upper troposphere. Furthermore, a dip in the correlation during June-July indicates a greater influence of the tropospheric latent heating owing to monsoon precipitation. On the other hand, the winter months show descending motion, but LST is still positively correlated with the overlying atmosphere, suggesting a strong land-atmosphere coupling during winter too.

3.3 Composite structures and plausible causes of WTP temperature anomaly

To corroborate the finding of a dominant mode in the Asian monsoon rainfall during June, composite analysis of precipitation during extreme WTP temperature years is done. Here, WTP averaged dtrended temperature anomaly $\geq|0.5|^{\circ} C$ during May is considered as the extreme year (red and blue bars in Fig. 7a; Table 1). We note that WTP temperature has a relatively weak association with Niño3.4 temperature during May, which is also true for the extreme years (Fig. 7b). There is a total of 33 (31) years with positive (negative) extreme WTP temperature anomalies during the last 115 years (1901–2015) of observations. Therefore, first 31 years of anomaly used for composite analysis. Neither the correlation between WTP temperature and Niño3.4 SST is strong ($r = -0.06$), nor the one-to-one correspondence between intense/extreme years of WTP temperature and Niño3.4 SST is good. The difference in composites of positive and negative extreme year's June rainfall and May 2 m temperature are shown in Fig. 7c, d. It is interesting to see that the spatial structure of composite difference is

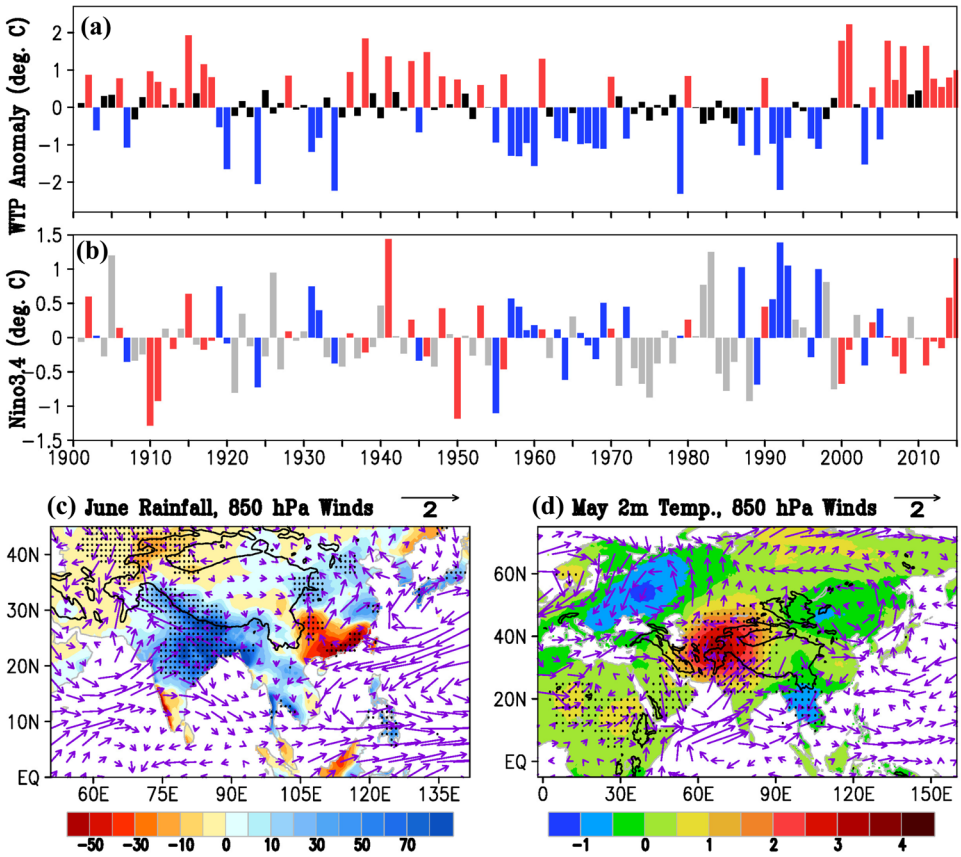

Fig. 7 A composite structure of monsoon rainfall during extreme WTP temperature years. **a** WTP average 2 m temperature anomaly and **b** Niño3.4 anomaly during May. WTP anomaly ≥ 0.5 (≤ −0.5) are marked by red(blue) color. Niño3.4 anomalies in sub-panel **b** are marked by corresponding colours in WTP. Composite difference (positive minus negative WTP anomaly for years WTP ≥| 0.50 |° *C*) in **c** rainfall (shaded; in mm) and 850 hPa winds (in m/s) during June, **d** 2 m air temperature (shaded; in °C) and 850 hPa winds (in m/s) during May. The differences in rainfall and temperature significant at 95% are stippled

very similar to that of EOF1. Similarly, there is no such area other than WTP with high-temperature differences. The low-level (850 hPa) composite difference in winds also suggests enhanced monsoon circulation in the south and east Asian regions. A strong cyclonic (weak anticyclonic) circulation anomaly is seen over the north of the Yangtze River and Bay of Bengal (south of the Yangtze river) during May, which also persists in the next month (i.e. June) in a pretty similar pattern. These indicate the role of local feedback processes (e.g. mountain, snow, glacier) in maintaining high surface temperature anomalies. It is plausible that global predictors modulate the atmospheric conditions around the WTP regions, and thereafter, in the presence of high mountains, the local feedback, such as snow-albedo, may retain the signal for a while. Land surface with snow and without snow (snow albedo can be as high as 0.9) can make huge difference in the net surface energy fluxes, which can affect the troposphere through change in sensible heat flux. A strong correlation (r=−0.65) between WTP averaged temperature and SWE using 70 years of data suggests such a possibility. Furthermore, the mean and inter-annual variability of SWE during May is higher around the WTP region than in the eastern TP (Figure S6a, b). Nevertheless, PC1 is positively correlated with SWE over some part the eastern TP (Figure S6c), which implies that May LST of the eastern TP is inversely (directly) related to June precipitation of North (South) of the Yangtze river, is consistent with earlier studies. (e.g. Xue et al. 2018). The occurrence of snow/temperature anomaly over TP may be a chaotic phenomenon or through the global predictors (evolves on inter-annul to multi-decadal time scale) in a predictable manner. In either case, the land surface may retain memory, which may affect the following monsoon rainfall.

At 0–3 months lead time, surface temperature (land and ocean) over the regions of major global predictors (i.e. AMO, PDO, IOD, Niño3.4, NAO) show significant correlations with May WTP LST (Figure S5). Since, the southern Indian ocean region also show a significant correlation, SST time series averaged over Indian Ocean Box (IOB) is also used as a predictor. Therefore, to explore the possibility of WTP temperature being associated with major global oceanic predictors, multiple regression of PC1 (June) and WTP (May) with six major predictors at lead/lag months is done (Fig. 8). Furthermore, PC1 is regressed with the lead/lag months of WTP averaged temperature (black curves in Fig. 8a, b). Here all the regression coefficients presented are standardized. PC1 is strongly and significantly associated with the WTP averaged temperature only during April and May. On the other hand, WTP temperature in May has a strong association with IOB and AMO during all lead/

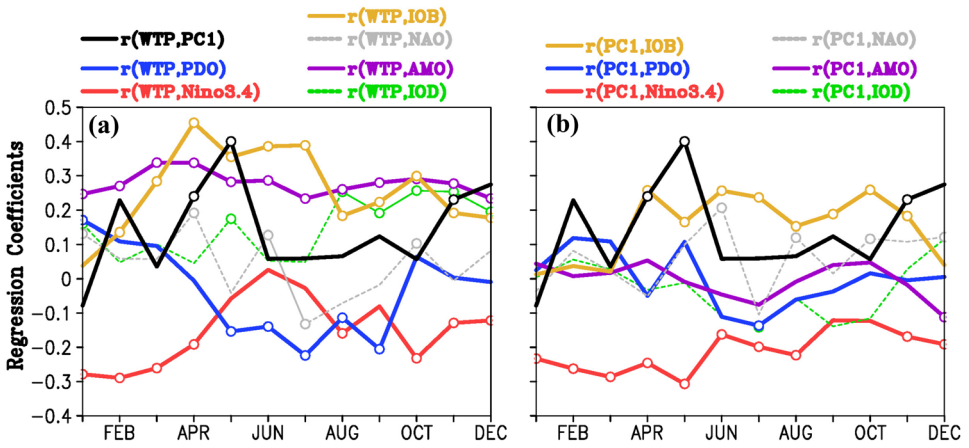

Fig. 8 Lead-lag relationship of WTP surface temperature and PC1 with global predictors. PC1 of June rainfall is regressed with WTP averaged temperature during all the lead/lag months (black lines in **a** & **b**). The global oceanic modes of the predictors (AMO, PDO, IOD, Niño3.4, NAO, IOB) in all months (i.e. January to December) are regresses (i.e. multiple regression) with **a** WTP averaged temperature during May, and **b** PC1 of June rainfall. Open circles represent regressions significant at 95% level using two-tailed Student's t-test (all regression coefficients are standardized)

lag months. Moreover, significant regression values with Niño3.4 during lead/lag months also suggest a possible role of ENSO in modulating WTP land surface conditions during winter and Autumn. It is also important to note that, in general, ENSO starts growing at the end of the summer season and peaks during winter, which may leave a signature in terms of snow/ice anomaly over the WTP region. The lead/lag relationship with PDO is also evident, but the amplitude is weak as compared to that of AMO and Niño3.4. As ENSO is known as the single largest predictor of the Asian summer monsoon, PC1 has the strongest association with Niño3.4 index, while the weaker association of the other Oceanic predictors suggests their indirect role (through a change in WTP land-surface conditions) on the initial phase of the Asian monsoon. The weaker role of WTP temperature (despite the strong association with AMO, IOB) in the following monsoon months (i.e. July to September) may be due to the much stronger convective feedback in maintaining a stronger tropospheric temperature gradient in association with global Oceanic predictors.

Table 1 Positive ($\geq 0.5\,^{\circ}C$) and negative ($\leq -0.5\,^{\circ}C$) anomaly years based on dtrended WTP averaged land surface temperature anomaly (2m air temperature)

Positive years	Negative years
1902 1906 1910 1911 1913	1903 1907 1919 1920 1924 1931
1915 1917 1918 1928 1936	1932 1934 1945 1955 1957 1958
1938 1941 1944 1946 1948	1959 1960 1963 1964 1966 1967
1950 1953 1956 1961 1970	1968 1969 1972 1979 1987 1989
1980 1990 2000 2001 2004	1991 1992 1993 1996 1997 2003
2006 2007 2008 2011 2012	2005
2013 2014 2015	

We recall a negative correlation between PC1 and 2 m temperature of May over the ICP region, resulting from cooling (warming) of the surface due to increased (decreased) rainfall (Fig. 3b). Moreover, enhanced convection over the Bay of Bengal and ICP region during pre-monsoon (i.e. during May) may trigger stationary Rossby wave train (e.g. Joseph and Srinivasan 1999), and that can influence the WTP temperature anomaly. To estimate a precise lead/lag time between convection and its response, we have used daily time series of precipitation and 2 m air temperature over ICP and WTP region respectively. A smooth annual cycle (sum of first three harmonics and mean) of daily WTP and ICP averaged temperature and rainfall respectively is constructed (Fig. 9). The daily tendency of precipitation and temperature is calculated using central difference scheme. The climatological mean and tendency suggest that WTP temperature begin to rise rapidly by more than a month ahead of rainfall increase over the ICP region (Fig. 9a, d). The peak of WTP temperature tendency, which happens in March, clearly leads the rainfall tendency over ICP by about one and half months (i.e. peak in the last week of April). Similarly, the maxima of the tendency of WTP averaged temperature in the vertical levels shows a tilt towards the following months (Fig. 9c), suggesting tropospheric heating by land surface. However, during the withdrawal phase of the monsoon, the cooling tendency maxima at around 300 hPa is rapid owing to combined effects of the reduction in solar insolation (Sun moving towards southern hemisphere) and drop in heating due to decrease in rainfall. The daily anomaly of WTP averaged temperature is regressed with the daily ICP rainfall anomaly (January to May, i.e. 151 days;

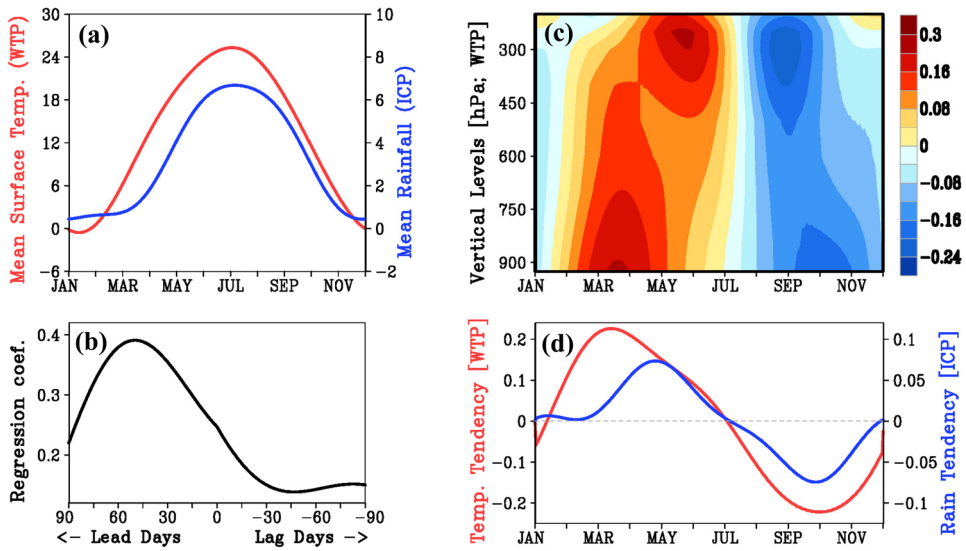

Fig. 9 Seasonal evolution of WTP and ICP averaged temperature and rainfall, respectively. **a** Smooth annual cycle of daily climatological mean temperature (red; CPC) and rainfall (blue; GPCP) averaged over WTP and ICP boxes, respectively (1997–2020). **b** Lead/lag regression of WTP temperature anomaly with ICP rainfall anomaly, where temperature leads the rainfall (regressed values are significant at above 99% level). **c** The mean vertical structure of the tendency of daily temperature averaged over WTP (ERA5; 1997–2020). **d** The average tendency of daily 2 m temperature (rainfall) over WTP (ICP) box. For the calculation of tendency/mean, the time series of the smooth annual cycle (first four harmonics) in each year is used

1979–2020, i.e. 42 years; a maximum sample size of about 6342). The daily anomalies are based on the smooth annual cycle, i.e. deviation of smooth annual cycles from the climatological mean annual cycle. It is noted that at the lead of WTP temperature by about 50 days, the regression coefficient is positive and maximum (significant more than 99%; Fig. 9b). Therefore, it is apparent that local heating is primarily responsible for the initial buildup of TTG anomaly, which in turn may have affected the pre-monsoon convection over the Bay of Bengal region.

4 WTP temperature teleconnection simulated by LS4P-I models

Now we use ensemble-averaged (8–10 ensembles) re-forecasted June rainfall and May surface temperature of 30 years (1981–2010) from five global coupled models (Table 2) available in LS4P-I to compare with the observed relationship. It is very important for the global forecast systems to be able to replicate the observed correlation between WTP averaged temperature during May and the first phase of monsoon rainfall faithfully.

Figure 10a show the observed correlation between WTP temperature during May and June rainfall over Asian continent regions for the years 1901–2019, which mimics the first EOF pattern. For recent past 30 years (1981–2010), this relationship has also held everywhere, except the region north and south of the Yangtze River (Fig. 10b). All the models show very good association over India (except IITM-CFS, which has a weak negative correlation; Fig. 10c–h). Furthermore, all the models, except ECMWF-IFS, fail to reproduce the correct sign over the Indochina peninsula. And none of the models shows observed signs in the regions north and south of the Yangtze River. Therefore, the multi-model average relation is quite good over India but fails to capture the observed pattern over Indochina peninsula, north and south of the Yangtze River.

The EOF analysis of June rainfall further reveals that all models fail to capture the observed phase relationship in the north and south of the Yangtze River and the ICP region (Fig. 11). While all models are able to capture the phase relationship over the south Asian region, the explained variance of EOF1 is stronger in all models than the observations, except in the IITM-CFS. The first mode in IITM-CFS is quite good as compared to the observations (Fig. 11a, b), but the other modes are equally problematic (Figure not shown). Therefore, in general, models have difficulties simulating the dominant rainfall variabilities, particularly over east Asia and ICP regions, which could be detrimental for sub-seasonal to seasonal prediction skill.

Now we examine the re-forecast skill of the models in 2 m air temperature against observations (i.e. merged CMA and CRU data described in see Sect. 2). Skilful simulation of spring temperature is crucial for a model to be able to capture the dominant mode or the first phase of the ASM rainfall. Gridpoint correlation skills between observations and models are shown in Fig. 12. All the models have

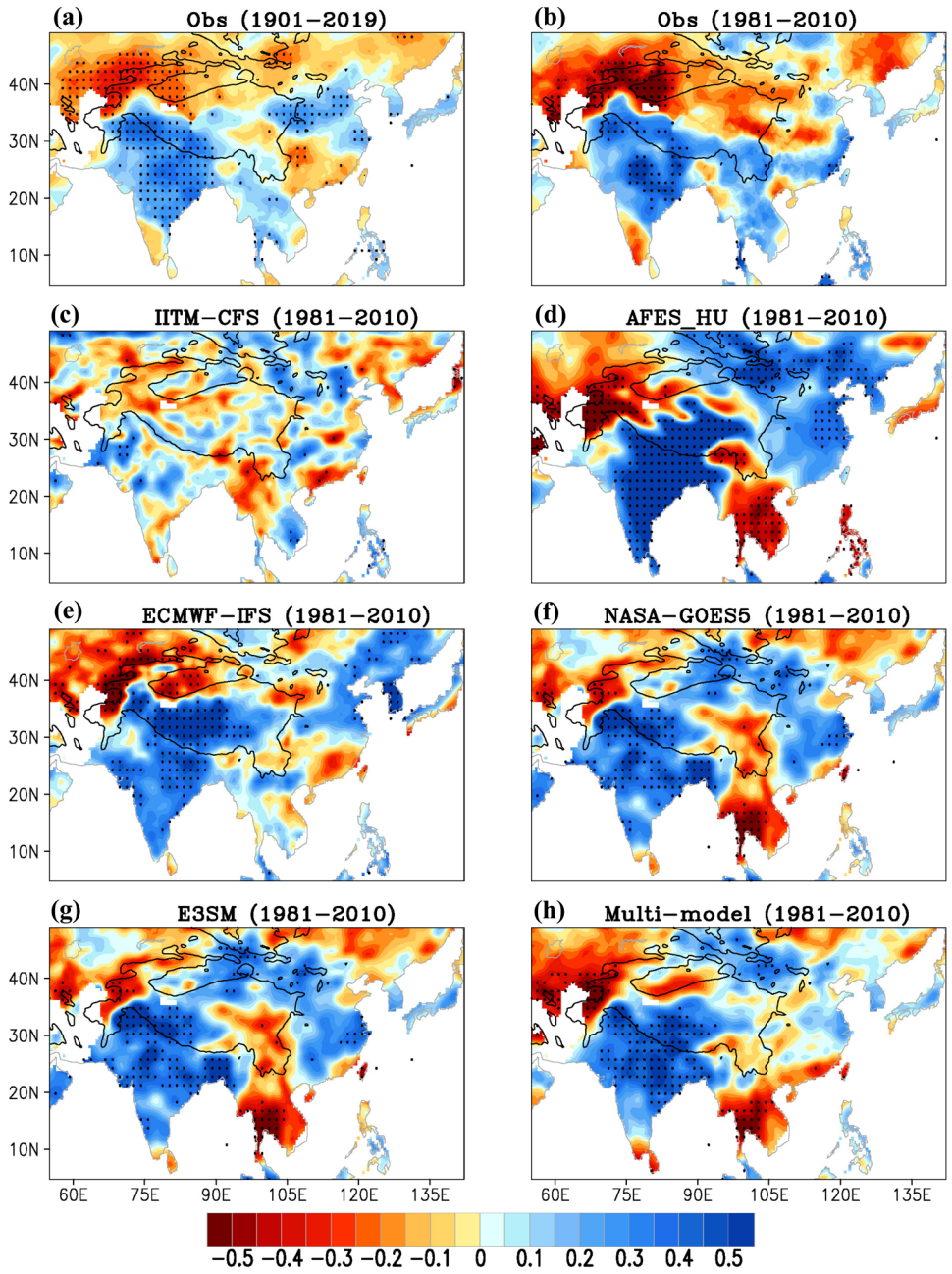

Fig. 10 Observed correlations between WTP averaged temperature during May and June rainfall in all grids for the year **a** 1901–2019, **b** 1981–2010, with CMA over China and CRU elsewhere. The same correlations for the year 1981–2010 were obtained from **c**IITM-CFS, **d** AFES-HU, **e** ECMWF-IFS, **f** NASA-GOES5, **g** E3SM, and **h** Multi-model average (five models). Correlations significant at 5% are stippled

serious difficulties in simulating the surface temperature of regions Northwest of the Mediterranean Sea. Over the WTP region, correlation skill varies between 0.24 to 0.85, while ECMWF-IFS shows the best skill all over the regions. We also note that using recent years data (1980–2015), Xue et al. (2018) have shown that a cold (warm) anomaly during May in eastern Tibet is associated with dry (wet) and wet (dry) rainfall anomaly during June over South and North of the Yangtze river respectively. Moreover, the EOF2 and EOF3 (Fig. 2), which have prominent dipole/tripole structures in the East Asian region, have a weak relationship with the WTP temperature.

Overall, the performance of models are rather poor in simulating 2 m temperature and its relationship with following month's precipitation. Even when models are initialized with obsetvations/reanalysis (soil and surface temperature), they quickly drift and are unable to retain the memory. The ILS4P group have collectively tried to understand the possible reasons. In fact, there are multiple reasons: a) bias in physical processes, b) soil properties (thermal and hydroulic) and relatively shallow depth of soil layer used in model, and c) uncertainty in the initial soil states (see Xue et al. 2021, 2022). Availability of reliable land snow and temperature (surface and sub-surface)

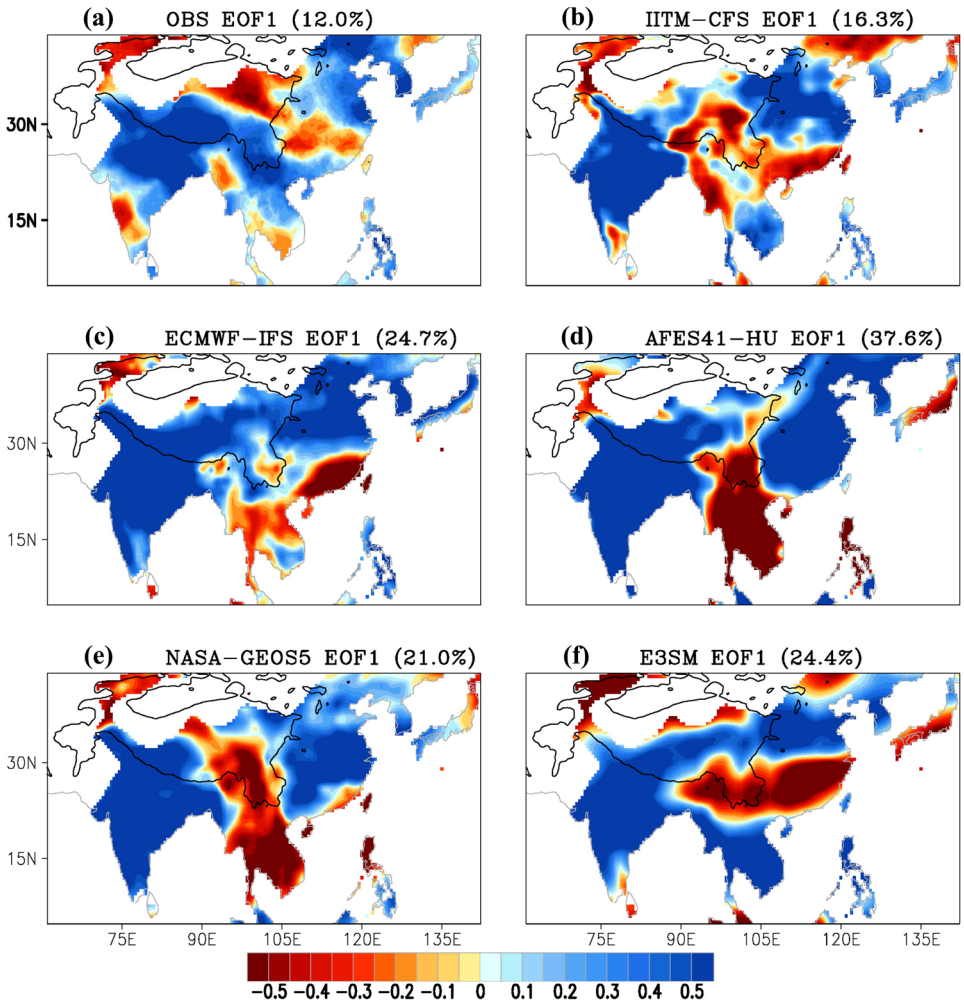

Fig. 11 EOF1 in June rainfall (1981–2010) from **a** CRU observations, **b** IITM-CFS, **c** ECMWF-IFS, **d** AFES-HU, **e** NASA-GOES5 and **f** E3SM

for initialization is a major issue owing to sparse observations (e.g. Xue et al. 2018).

5 Discussion and conclusion

The people of the south and east Asian region eagerly wait for the arrival of the summer monsoon rainfall. Arrival of the summer monsoon, which rejuvenates the entire ecosystem, is greeted and celebrated with joy in many parts of Asia. Nevertheless, the year-to-year variability in the initial phase of the Asian monsoon (May and June) is quite strong (Fig. 1c, d) compared to its seasonal counterpart. In south Asia, often, the weak (strong) initial phase of rainfall is associated with below (above) normal seasonal (June-to-September) rainfall (Kothawale and Kulkarni 2014). Therefore, the prediction of the initial phase of the Asian summer monsoon (ASM) rainfall has considerable societal and economic benefits.

Employing EOF analysis on 119 years of June (and May-June average) rainfall, we show that the first dominant mode explains 12% of the total variance and has a mono-pole structure over the Indian sub-continent, Indochina peninsula and a dipole structure between the regions north and south of the Yangtze River in China (Fig. 2). We found that PC1 is strongly correlated with the surface temperature of the western TP (WTP) region in May (by a maximum of 0.5 (0.65), using 119 years of June (May-June) rainfall). This region is also home to the second height mountain peak in the world. A large part of this region remains covered with snow and glaciers. Hence, the surface temperature strongly correlates with snow water equivalent over WTP during May ($r = 0.65$). It is shown that surface warming tendency over WTP begins in the early spring season, affecting the tropospheric temperature and hence the large-scale moisture fluxes in the following month of May and June over the Asian summer monsoon region.

While June rainfall over north (south) of the Yangtze River is inversely (directly) related to the May temperature of eastern TP (Xue et al. 2018), our results show opposite effects of western TP temperature in May on the June rainfall over the same region. It is quite well known that western

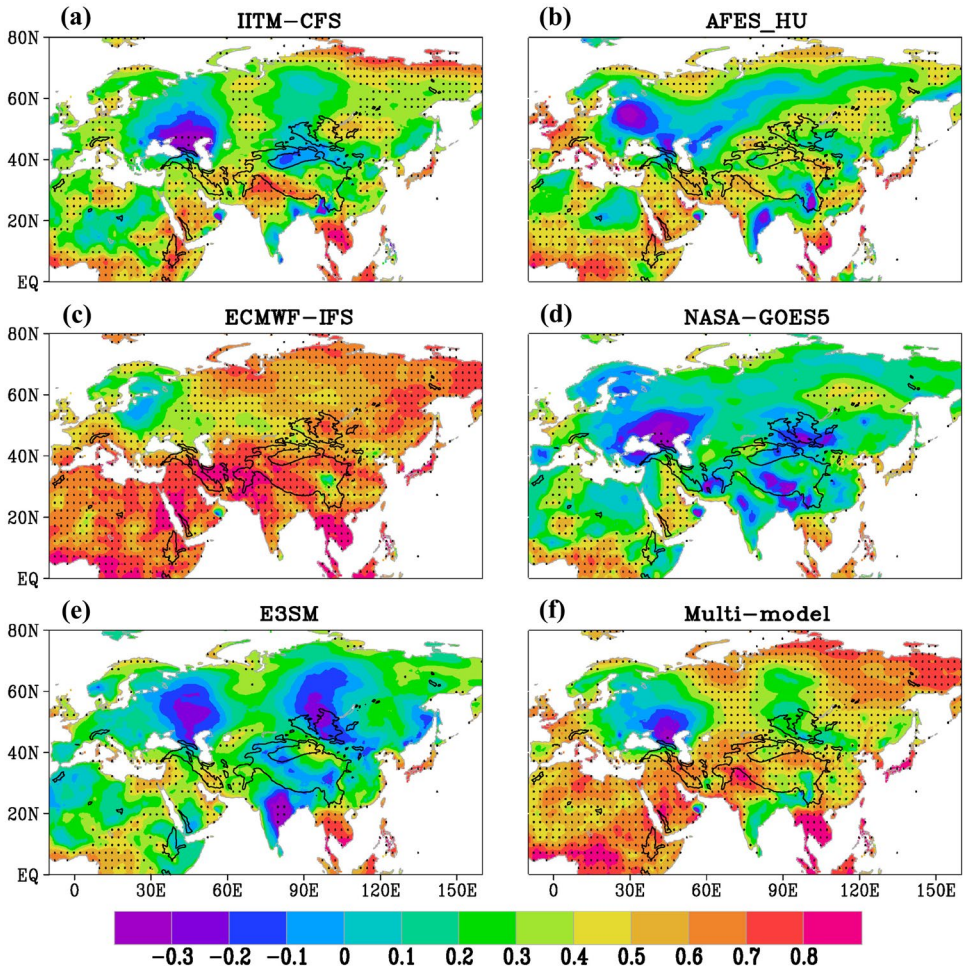

Fig. 12 Correlations between observed and model-simulated 2 m air temperature in May (1981–2010). **a** IITM-CFS, **b** AFES-HU, **c** ECMWF-IFS, **d** NASA-GOES5, **e** E3SM, and **f** Multi-model average (five models). Correlations significant at 95% using two-tailed Student's t-test are stippled (black dots)

Table 2 List of five Earth system models from LS4P-I used in this study

Model	Institute name	Atms. resolution	Convection scheme	PBL	Land surface
AFES-HU	Hokkaido University	T79 (~150 km)	Emanuel	Nonlocal	MATSIRO
Nakamura et al. (2015)	Japan	56 vertical levels	Convection	Boundary layer	
ECMWF-IFS	ECMWF	Tco199 (~25 km)	Tietdke scheme	McRad radiation	HTESSEL
Johnson et al. (2019)	United Kingdom	91 vertical levels	With several Improvements	Scheme	
E3SM	Lawrence livermore	1° × 1°	Shallow: CLUBB	CLUBB	ELMv0
Golaz et al. (2019)	National laboratory, USA		Deep: ZM		
IITM-CFS	IITM, Pune	T126 (~111 km)	Simplified	Nonlocal	NOAH
Saha et al. (2019)	India	64 vertical levels	Arakawa-Schubert (SAS)	Boundary layer	
NASA-GOES5	NASA Goddard space	T126 (~111 km)	KIM SAS (KSAS)	Scale-aware YSU	Revised
Molod et al. (2020)	Flight Center, USA	42 vertical levels			NOAH

and eastern TP have different heating characteristics (e.g. Ye and Gao 1979). In the case of the western Plateau, sensible heating dominates during spring, while for the eastern Plateau, condensation heating dominates after the monsoon onset. And this east–west contrast is likely to be related to the marked difference in the surface properties (e.g. Shi and Smith 1992). Hence, the effects of eastern and western TP may have different effects on the regional monsoon.

We have also used a re-forecast of 1981–2010 by five global models (8–10 ensemble average) to test their ability in simulating the observed relationship between May WTP temperature and June rainfall over the Asian monsoon region. Out of five models, four models are able to capture the observed relationship over south Asia, but all fails in the north and south of the Yangtze River. Moreover, over the Indochina peninsula, only ECMWF-IFS is closer to the observations. Apart from WTP regions, it is also equally important for models to reasonably simulate the spring surface temperature of the surrounding regions (i.e. Sahara, mid and high latitude regions) of the core Asian monsoon zone. We show that all models, except ECMWF-IFS, have serious difficulty in simulating May 2 m temperature. This study highlight importance of spring surface temperature in association with land surface processes on the prediction of the first phase of the ASM. In order to be skilful in predicting Asian monsoon rainfall, the model also should be skilful enough to capture antecedent land surface temperature. Land surface temperature of WTP region appears to be an important source of the Asian summer monsoon predictability. It may be noted that most of the major rivers in south and east Asia originated from the TP. Moreover, the TP region has witnessed warming in the recent past decades, which is unprecedented in the past 2000 years, leading to strong cryospheric melt and intensification of the water cycle. (Yao et al. 2019). Therefore, the natural variability of the initial phase of the monsoon may be affected by climate change, which may also have serious implications for the predictability of the monsoon in the future.

Supplementary Information The online version of this article (https://doi.org/10.1007/s00382-023-06709-7) contains supplementary material, which is available to authorized users.

Acknowledgements SKS, SK, HC and YS thank MoES, Government of India and Director IITM, for all the support to carry out this work.

Author contributions SKS and YX conceptualized the work, SK run the model, ID helped to setup experiments and managed model and observation data, YS and HC did data analysis, TN and QT provided data from their model reforecast experiments. All authors have contribute in writing the manuscript.

Funding IITM is funded by Ministry of Earth Sciences, Government of India. Ismaila Diallo was funded by the Center for Earth System Modeling, Analysis, and Data at The Pennsylvania State University. Energy Exascale Earth System Model (E3SM) project, funded by the U.S. Department of Energy (DOE), Office of Science, Office of Biological and Environmental Research (BER) under the auspices of the U.S. DOE by Lawrence Livermore National Laboratory under contract no. DE-C52-07NA27344. This research used resources of the National Energy Research Scientific Computing Center, a DOE Office of Science User Facility supported by the Office of Science of the U.S. DOE under contract no. DE-AC02-05CH11231.

Availability of data and materials All data used in this study are freely available. Gridded surface temperature and precipitation data from Climatic Research Unit Time Series (CRU TS; $0.5° \times 0.5°$; monthly) for 1901–2019 is used (Harris et al. 2020). The monthly indices of ENSO, PDO, AMO and IOD is obtained from the site https://psl.noaa.gov/data/climateindices/list/. Indian summer monsoon onset date over Kerala based on India Meteorological Department's (IMD's) subjective (1901–2005) and objective (1971–2019) criteria are taken from Preenu et al. (2017). Monthly gridded snow water equivalent (SWE) data for the period 1950–2019 from ERA-land reanalysis is utilized (Muñoz Sabater et al. 2021). Monthly geopotential height data at 200 & 500 hPa (1901–2015) are from 20th Century Reanalysis V3 data by the NOAA/OAR/ESRL PSL, Boulder, Colorado, USA, from their Web site at https://psl.noaa.gov/data/gridded/data.20thC_ReanV3.html. The daily pressure level atmospheric temperature is from ERA5 reanalysis (1997–2020; Hersbach et al. 2020). CPC daily global temperature data provided by the NOAA/OAR/ESRL PSL, Boulder, Colorado, USA, from their Web site at https://psl.noaa.gov/data/gridded/data.cpc.globaltemp.html is used for 1997–2020. Daily rainfall data from GPCP (Bolvin et al. 2009) for the period 1997–2020 is used.

Code availability All code and scripts are available on request from the corresponding author.

Declarations

Conflict of Interest No conflict of interest with funding agency, reviewer, editors or any individual/organizations.

Ethical approval This work is not published elsewhere in any form or language. Freely available software (GrADS, Fortran) are used..

Consent to participate Not applicable.

Consent to publications All authors/co-authors have given consent for publication of this work.

References

Adler RF, Huffman GJ, Chang A et al (2003) The version 2 global precipitation climatology project (gpcp) monthly precipitation analysis (1979- present). J Hydrometeor 4:1147–1167

Asharaf S, Ahrens B (2013) Soil-moisture memory in the regional climate model COSMO-CLM during the Indian summer monsoon season. J Geophys Res 118(12):6144–6151. https://doi.org/10.1002/jgrd.50429

Bamzai AS, Shukla J (1999) Relation between Eurasian Snow Cover, Snow Depth, and the Indian Summer Monsoon: an observational study. J Clim 12:3117–3132

Blanford HF (1884) On the connection of the Himalayan snowfall with dry winds and seasons of droughts in India. Proc Roy Soc London 37:3–22

Bolvin DT, Adler RF, Huffman GJ et al (2009) Comparison of GPCP monthly and daily precipitation estimates with high-latitude gauge observations. J Appl Meteorol Climato 48(9):1843–1857. https://doi.org/10.1175/2009JAMC2147.1

Boos W, Kuang Z (2010) Dominant control of the South Asian monsoon by orographic insulation versus plateau heating. Nature 463:218–222. https://doi.org/10.1038/nature08,707

Charney JG, Shukla J (1981) Predictability of monsoons. In: Lighthill J, Pearce RP (eds) Monsoon Dyn. Cambridge University Press, Cambridge, pp 99–108

Diallo I, Xue Y, Li Q et al (2019) Dynamical downscaling the impact of spring Western US land surface temperature on the 2015 flood extremes at the Southern Great Plains: effect of domain choice,

dynamic cores and land surface parameterization. Clim Dyn 53:1039–1061. https://doi.org/10.1007/s00382-019-04630-6
Diallo I, Xue Y, Chen Q et al (2022) Effects of spring Tibetan Plateau land temperature anomalies on early summer floods/droughts over the monsoon regions of South East Asia. Clim Dyn. https://doi.org/10.1007/s00382-021-06053-8
Dong B, Valdes PJ (1998) Modelling the Asian summer monsoon rainfall and Eurasian winter/spring snow mass. Q J R Meteorol Soc 123:2567–2596
Golaz JC, Caldwell PM, Van Roekel LP et al (2019) The DOE E3SM coupled model version 1: overview and evaluation at standard resolution. J Adv Model Eart Syst 11(7):2089–2129. https://doi.org/10.1029/2018MS001603
Goswami BN (2012) South Asian monsoon. chapt. 2. In: Lau WKM, Waliser DE (eds) Intraseasonal Var Atmos Ocean Clim Sys. Praxis, Springer, Berlin, Heidelberg, pp 131–201
Goswami BN, Xavier PK (2005) Dynamics of internal interannual variability of the Indian summer monsoon in a GCM. J Geophys Res 110(D24):104. https://doi.org/10.1029/2005JD006,042
Han S, Shi C, Xu B et al (2019) Development and evaluation of hourly and kilometer resolution retrospective and real-time surface meteorological blended forcing dataset (SMBFD) in China. J Meteor Res 33:1168–1181. https://doi.org/10.1007/s13351-019-9042-9
Harris I, Osborn TJ, Jones P et al (2020) Version 4 of the CRU TS monthly high-resolution gridded multivariate climate dataset. Sci Data 7(109):56. https://doi.org/10.1038/s41597-020-0453-3
Hersbach H, Bell B, Berrisford P et al (2020) The ERA5 global reanalysis. Q J R Meteorol Soc 146(730):1999–2049. https://doi.org/10.1002/qj.3803
Johnson SJ, Stockdale TN, Ferranti L et al (2019) SEAS5: the new ECMWF seasonal forecast system. Geosc Model Devel 12(3):1087–1117
Joseph PV, Srinivasan J (1999) Rossby waves in may and the Indian summer monsoon rainfall. Tellus A 51(5):854–864
Kothawale DR, Kulkarni JR (2014) Performance of all-India southwest monsoon seasonal rainfall when monthly rainfall reported as deficit/excess. Met Appli 21(3):619–634. https://doi.org/10.1002/met.1385
Kripalani RH, Kulkarni A (1999) Climatology and variability of historical Soviet snow depth data: some new perspectives in snow-Indian monsoon teleconnections. Clim Dyn 15:475–489
Krishnamurthy V, Shukla J (2000) Intraseasonal and interannual variability of rainfall over India. J Clim 13:4366–4377
Luo M, Lin L (2017) Objective determination of the onset and withdrawal of the South China Sea summer monsoon. Atmos Sci Let 18(6):276–282. https://doi.org/10.1002/asl.753
Mao J, Chan JCL (2004) Relationship between the Onset of the South China Sea Summer Monsoon and the Structure of the Asian Subtropical Anticyclone. J Meteor Soc Jap 82(3):845–849
Molod A, Hackert E, Vikhliaev Y et al (2020) GEOS-S2S version 2: the GMAO high-resolution coupled model and assimilation system for seasonal prediction. J Geophys Res 125(5):e2019JD031. https://doi.org/10.1029/2019JD031767
Muñoz Sabater J, Dutra E, Agustí-Panareda A et al (2021) Era5-land: a state-of-the-art global reanalysis dataset for land applications. Earth Syst Sci Data 13(9):4349–4383
Nakamura T, Yamazaki K, Iwamoto K et al (2015) A negative phase shift of the winter AO/NAO due to the recent Arctic sea-ice reduction in late autumn. J Geophys Res 120(8):3209–3227. https://doi.org/10.1002/2014JD022848
North G, Bell T, Cahalan R et al (1982) Sampling erors in the estimation of empirical orthogonal functions. Mon Weather Rev 110(7):706. https://doi.org/10.1175/1520-0493(1982)110<0699:SEITEO>2.0.CO;2
Pai DS, Bandgar A, Devi S et al (2020) Normal dates of onset/progress and withdrawal of southwest monsoon over India. Mausam 71(4):553–570. https://doi.org/10.54302/mausam.v71i4.33
Preenu PN, Joseph PV, Dineshkumar PK (2017) Variability of the date of monsoon onset over Kerala (India) of the period 1870–2014 and its relation to sea surface temperature. J Earth Syst Sci 126(76):1–9. https://doi.org/10.1007/s12040-017-0852-9
Qian W, Lee DK (2000) Seasonal march of asian summer monsoon. J Royal Meterol Soc 20(11):1371–1386. https://doi.org/10.1002/1097-0088(200009)20:11<1371::AID-JOC538>3.0.CO;2-V
Rai A, Saha SK, Pokhrel S et al (2015) Influence of preonset land atmospheric conditions on the Indian summer monsoon rainfall variability. J Geophys Res 120(17):8783–803. https://doi.org/10.1002/2015JD023,159
Ringler TD, Cook KH (1999) Understanding the seasonality of orographically forced stationary waves: Interaction between mechanical and thermal forcing. J Atmos Sci 56(9):1154–1174. https://doi.org/10.1175/1520-0469(1999)056<1154:UTSOOF>2.0.CO;2
Robock A, Vinnikov KY, Srinivasan G et al (2000) The global soil moisture data bank. Bul Amer Meteor Soc 81(6):1281–1300
Rodwell MJ, Hoskins B (1966) Monsoons and the dynamics of deserts. Q J R Meteorol Soc 122:1385–1404
Rosenzweig MR, Binswanger HP (1993) Wealth, weather risk and the composition and profitability of agricultural investments. Econ J 103:56–78. https://doi.org/10.2307/2234337
Saha SK, Halder S, Kumar KK et al (2011) Pre-onset land surface processes and 'internal' interannual variabilities of the Indian summer monsoon. Clim Dyn 36:2077–2089
Saha SK, Halder S, Rao AS et al (2012) Modulation of ISOs by land-atmosphere feedback and contribution to the interannual variability of Indian summer monsoon. J Geophys Res 117(D13):101. https://doi.org/10.1029/2011JD017,291
Saha SK, Pokhrel S, Chaudhari HS (2013) Influence of Eurasian snow on Indian summer monsoon in NCEP CFSv2 freerun. Clim Dyn 41:1801–1815
Saha SK, Sujith K, Pokhrel S et al (2016) Predictability of global monsoon rainfall in NCEP CFSv2. Clim Dyn 47:1693–1715
Saha SK, Sujith K, Pokhrel S et al (2017) Effects of multilayer snow scheme on the simulation of snow: Offline Noah and coupled with NCEP CFSv2. J Adv Model Eart Syst 9:271–290
Saha SK, Hazra A, Pokhrel S et al (2019) Unraveling the mystery of Indian summer monsoon prediction: Improved estimate of predictability limit. J Geophys Res 124:1962–1974
Saha SK, Hazra A, Pokhrel S et al (2020) Reply to comment by E. T. Swenson, D. Das, and J. Shukla on 'Unraveling the mystery of Indian summer monsoon prediction: improved estimate of predictability limit''. J Geophys Res 125:e2020JD033.
Saha SK, Konwar M, Pokhrel S et al (2021) Interplay between subseasonal rainfall and global predictors in modulating interannual to multidecadal predictability of the ISMR. Geophys Res Lett 48:e2020GL091. https://doi.org/10.1029/2020GL091,458
Senan R, Orsolini YJ, Weisheimer A et al (2016) Impact of springtime Himalayan-Tibetan Plateau snowpack on the onset of the Indian summer monsoon in coupled seasonal forecasts. Clim Dyn 47:2709–2725. https://doi.org/10.1007/s00382-016-2993-y
Shi L, Smith EA (1992) Surface forcing of the infrared cooling profile over the Tibetan Plateau. Part II: cooling-rate variation over large-scale plateau domain during summer monsoon transition. J Atmos Sci 49:823–844
Shukla J (1981) Dynamical predictability of monthly means. J Atmos Sci 38:2547–2572
Shukla J (1998) Predictability in the midst of chaos: A scientific basis for climate forecasting. Science 282:728–731
Shukla J (2007) Monsoon mysteries. Science 318:204–205

Subash N, Gangwar B (2014) Statistical analysis of Indian rainfall and rice productivity anomalies over the last decades. Int J Climatol 34:2378–2392. https://doi.org/10.1002/joc.3845

Wang B, LinHo Zhang Y et al (2004) Definition of south china sea monsoon onset and commencement of the east asia summer monsoon. J Clim 17(4):699–710. https://doi.org/10.1175/2932.1

Wang B, Liu J, Kim H et al (2012) Recent change of the global monsoon precipitation (1979–2008). Clim Dyn 39:1123–1135

Wang B, Li J, Cane MA et al (2018) Toward predicting changes in the land monsoon rainfall a decade in advance. J Clim 31(7):2699–2714

WMO (2013) Sub-seasonal to Seasonal Prediction: Research implementation plan. WMO Technical Report, World Meteorological Organisation, Geneva, https://library.wmo.int/index.php?lvl=notice_display &id=15820#.YfunoqbhWHs

Wu RG (2017) Relationship between Indian and East Asian summer rainfall variations. Advanc Atms Sc 34(1):4–15. https://doi.org/10.1007/s00376-016-6216-6

Xavier PK, Marzin C, Goswami BN (2007) An objective definition of the Indian summer monsoon season and a new perspective on the ENSO-monsoon relationship. Q J R Meteorol Soc 133:749–764

Xue Y, Oaida CM, Diallo I et al (2016) Spring land temperature anomalies in northwestern US and the summer drought over Southern Plains and adjacent areas. Env Res Let 117:044018. https://doi.org/10.1088/1748-9326/11/4/044018

Xue Y, Diallo I, Li W et al (2018) Spring land surface and subsurface temperature anomalies and subsequent downstream late spring-summer droughts/floods in North America and East Asia. J Geophys Res 123(10):5001–5019. https://doi.org/10.1029/2017JD028246

Xue Y, Diallo I, Boone AA et al (2022) Spring land temperature in Tibetan Plateau and global-scale summer precipitation - initialization and improved prediction. Bul Amer Meteor Soc. https://doi.org/10.1175/BAMS-D-21-0270.1

Xue Y, Vasic R, Janjic Z et al (2012) The impact of spring subsurface soil temperature anomaly in the western U.S. on North American summer precipitation: A case study using regional climate model downscaling. J Geophys Res 117:D11. https://doi.org/10.1029/2012JD017692

Xue Y, Yao T, Boone AA et al (2021) Impact of initialized land surface temperature and snowpack on subseasonal to seasonal prediction project, Phase I (LS4P-I): organization and experimental design. Geosc Model Devel 14(7):4465–4494

Yanai M, Wu GX (2006) Effects of Tibetan Plateau. In: Wang B (ed) The Asian Monsoon. Praxis, Springer, Berlin, pp 513–549

Yanai M, Li C, Song Z (1992) Seasonal Heating of the Tibetan Plateau and Its Effects on the Evolution of the Asian Summer Monsoon. J Meteorol Soc Jpn Ser II 70(1B):319–351. https://doi.org/10.2151/jmsj1965.70.1B_319

Yang S, Lau WKM (2006) Interannual variability of the Asian Monsoon. In: Wang B (ed) The Asian Monsoon. Praxis, Springer, Berlin, pp 259–293

Yao T, Xue Y, Chen D et al (2019) Recent third pole's rapid warming accompanies cryospheric melt and water cycle intensification and interactions between monsoon and environment: Multidisciplinary approach with observations, modeling, and analysis. BAMS 100(3):423–444. https://doi.org/10.1175/BAMS-D-17-0057.1

Ye DZ, Gao DY (1979) The influence on the atmosphere of the heating of Mount Qomolangma during spring and summer. Report of Science Expedition on Mount Qomolangma (1975), Meteorology and Environment, Chinese Science Press

Yihui D, Chan JCL (2005) The East Asian summer monsoon: an overview. Meteor Atmos Phys 89:117–142

Zhang R, Zhang R, Zuo Z (2017) Impact of Eurasian spring snow decrement on east asian summer precipitation. J Clim 30(9):3421–3437